

Two Novel Deep-Ultraviolet Nonlinear Optical Crystals with Shorter Phase-Matching Second Harmonic Generation than $\text{KBe}_2\text{BO}_3\text{F}_2$: A First-Principles Prediction

Lei Kang, Fei Liang, Pifu Gong, Zheshuai Lin,* Feng Liu,* and Bing Huang*

In this work, we propose a strategy to design new deep-ultraviolet (deep-UV) nonlinear optical (NLO) materials through the combination of borate and phosphate NLO material genome. Accordingly, a series of borophosphates are predicted with very large energy bandgaps, strong second harmonic generation (SHG) effects, and moderate birefringence in the deep-UV region. In particular, two novel fluoride borophosphates, PBO_3F_2 and $\text{PB}_3\text{O}_6\text{F}_2$, are able to achieve the deep-UV SHG laser output with shorter phase-matching wavelengths (≈ 155 and 137 nm) than that of $\text{KBe}_2\text{BO}_3\text{F}_2$ (KBBF, ≈ 161 nm). Further calculations show that these two structures are dynamically and thermodynamically stable, thus triggering possible synthesis, growth, and applications of them. The results attest that the proposed strategy is instructive and pave a comprehensive road map for us to discover new NLO crystals, especially in the borophosphate catalog with excellent deep-UV phase-matching capabilities beyond KBBF.

Deep-ultraviolet (deep-UV) nonlinear optical (NLO) crystals with short second harmonic generation (SHG) output wavelength and high frequency conversion efficiency are of great importance for current and future basic research and technology demands.^[1] Up to date, $\text{KBe}_2\text{BO}_3\text{F}_2$ (KBBF) is the sole practical NLO material that possesses excellent sixth-harmonic output capacity in deep-UV region, although its conversion power for practical 177.3 nm laser is still below watt-level (≈ 200 mW).^[2] Therefore, in the field of deep-UV laser technology one of the most important issues is to design new deep-UV NLO materials with shorter SHG output

wavelength and higher operating power than those of KBBF. The achievement of the phase-matching condition is the key to solve this problem and guarantee a NLO output with a sufficient efficiency and suitable wavelength, which is a very important requirement for the practical NLO process.^[3] In this sense, many materials with large deep-UV bandgaps and strong NLO effects actually cannot achieve an effective deep-UV output, due to their weak phase-matching abilities.^[4] BPO_4 (space group $I4$) is such a typical material, in which both boron and phosphorus atoms are tetrahedral coordinated (see Figure 1a).^[5] This material possesses a very strong SHG effect (≈ 0.76 pm V^{-1}), 1.5 times larger than d_{16} ≈ 0.45 pm V^{-1} of KBBF,^[2] and a very short deep-UV absorption edge (≈ 134 nm, or bandgap


≈ 9.3 eV),^[4] almost the shortest among all known NLO borates.^[4] However, BPO_4 cannot achieve the deep-UV phase-matching SHG output due to its relatively small optical birefringence (< 0.01).^[6] According to the anionic group theory, the reason comes from the small structural anisotropy of the NLO-active $(\text{BO}_4)^{5-}$ and $(\text{PO}_4)^{3-}$ tetrahedral anionic units in BPO_4 , which results in a small optical anisotropy of the whole system.^[7] Consequently, it cannot satisfy the phase-matching requirement by compensating the dispersion of refractive indices along different optical principle axis (i.e., birefringence is too small). Similar case is LiB_3O_5 ,^[11] in which the small birefringence (≈ 0.04) results in its limited phase-matching wavelength to be only 255 nm. Therefore, if a material (e.g., BPO_4) with a good deep-UV transparency is expected to be a phase-matching deep-UV NLO material, its structural anisotropy has to be enhanced.

With the development of density functional theory (DFT) and Materials Genome Initiative,^[8] under the guidance of basic physical and chemical principles, high-performing theoretical simulations have become an effective and efficient method to design and evaluate new NLO materials that have not been found in experiments.^[9] Basically, there are mainly four NLO-active anionic units (or so-called NLO material genome) in borates, i.e., $(\text{B}_3\text{O}_6)^{3-}$ (e.g., in $\beta\text{-BaB}_2\text{O}_4$),^[10] $(\text{B}_3\text{O}_7)^{5-}$ (e.g., in LiB_3O_5),^[11] $(\text{BO}_3)^{3-}$ (e.g., in KBBF),^[2] and $(\text{BO}_4)^{5-}$ (e.g., in BPO_4),^[5] exhibiting a desirable structural chemistry with a great variety of connection and arrangement patterns.^[12] Many studies have been contributed to elucidate the structure–property relationship

Dr. L. Kang, Prof. B. Huang
Beijing Computational Science Research Center
Beijing 100193, China
E-mail: bing.huang@csr.ac.cn

Dr. L. Kang, Prof. F. Liu
Department of Materials Science and Engineering
University of Utah
UT 84112, USA
E-mail: fliu@eng.utah.edu

Dr. F. Liang, Dr. P. Gong, Prof. Z. Lin
Technical Institute of Physics and Chemistry
Chinese Academy of Sciences
Beijing 100190, China
E-mail: zslin@mail.ipc.ac.cn

 The ORCID identification number(s) for the author(s) of this article can be found under <https://doi.org/10.1002/pssr.201800276>.

DOI: 10.1002/pssr.201800276

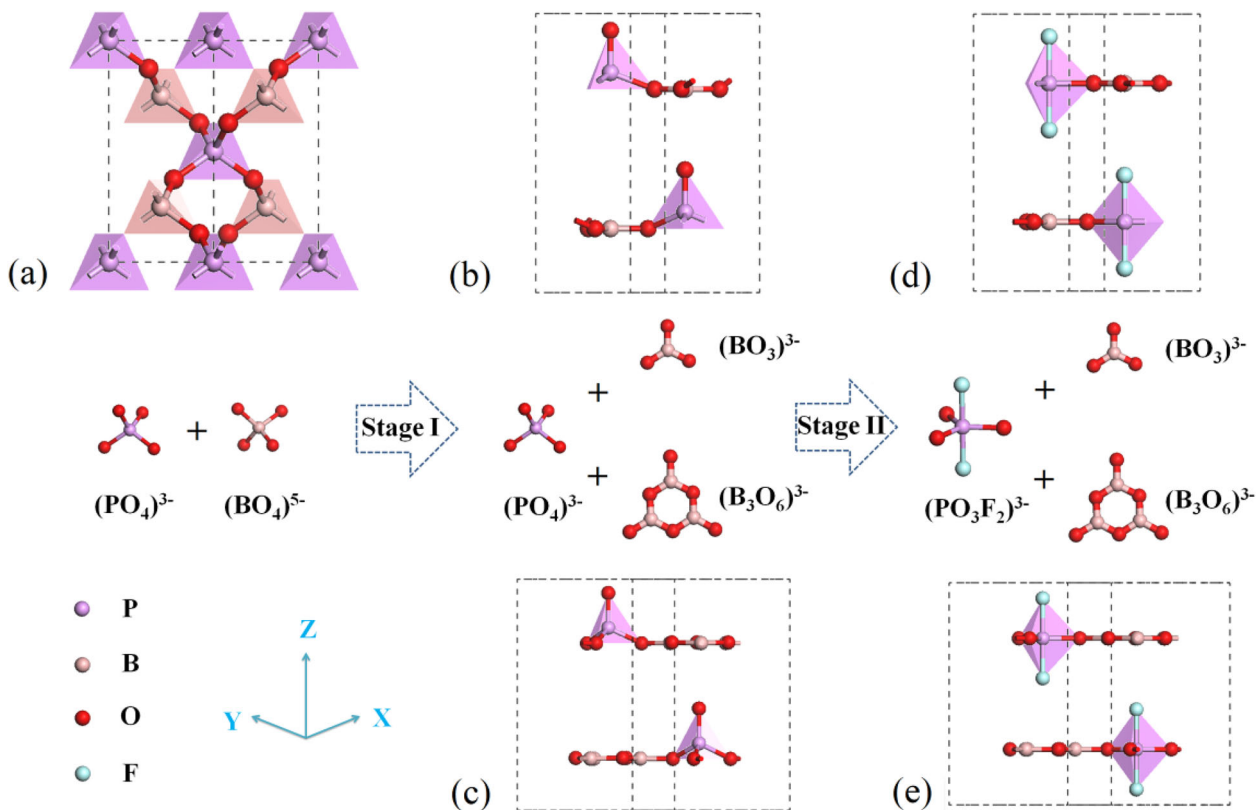


Figure 1. Schematic diagram of structure evolution from (a) BPO₄ to (b) PBO₃O and (c) PB₃O₆O (stage I) and then to (d) PBO₃F₂ and (e) PB₃O₆F₂ (stage II).

in borates based on the anionic group theory proposed by Chen, thus revealing that the micro-birefringence Δn and energy bandgaps E_g (exactly, HOMO-LUMO gap) of the four typical borate anionic units obey the following relative orders (per unit volume)^[7]:

$$\Delta n(\text{B}_3\text{O}_6) > \Delta n(\text{B}_3\text{O}_7) > \Delta n(\text{BO}_3) \gg \Delta n(\text{BO}_4)$$

$$E_g(\text{BO}_4) > E_g(\text{BO}_3) \approx E_g(\text{B}_3\text{O}_7) > E_g(\text{B}_3\text{O}_6)$$

Note that the $(\text{BO}_3)^{3-}$, $(\text{B}_3\text{O}_6)^{3-}$, and $(\text{B}_3\text{O}_7)^{5-}$ units exhibit relatively larger Δn compared to $(\text{BO}_4)^{5-}$ because they exhibit much larger planar anisotropy of polarization than the tetrahedron. Among them, however, $(\text{B}_3\text{O}_7)^{5-}$ groups have been proven negatively to construct in a layered framework so that the planar components are not arranged in a largely anisotropic form. This is the structural reason why LiB₃O₅ has a small birefringence (≈ 0.04), in which the $(\text{B}_3\text{O}_7)^{5-}$ groups link with each other to form the endless helices of $(\text{B}_3\text{O}_7)_{n \rightarrow \infty}$ chains along the crystal *c*-axis.^[11] Therefore, to significantly increase the structural anisotropy, herein, we introduce the coplanar $(\text{BO}_3)^{3-}$ or $(\text{B}_3\text{O}_6)^{3-}$ units with conjugated π orbitals instead of $(\text{BO}_4)^{5-}$ to coordinate with the $(\text{PO}_4)^{3-}$ unit in BPO₄, hence forming a perfect two-dimensional layered framework structure. This rational design strategy not only increases the structural anisotropy significantly but also enlarges the bandgap of compounds since the three dangling bonds on terminal oxygen

atoms of $(\text{BO}_3)^{3-}$ or $(\text{B}_3\text{O}_6)^{3-}$ are eliminated by adjacent P atoms.^[13] Then, fluorine atoms are incorporated into the lattice to further eliminate the nonbonding states and tune the construction of the basic units as an effective structural terminator.^[14] According to this strategy, in this work, a series of borophosphates are designed and evaluated as the possible deep-UV NLO crystals based on the DFT calculations.

The DFT calculations are performed using the plane-wave pseudopotential method implemented in the CASTEP package.^[15] The ion–electron interactions are modeled by the optimized norm-conserving pseudopotentials for all constituent elements.^[16] A kinetic energy cutoff of 850 eV is chosen with Monkhorst-Pack *k*-point meshes spanning less than 0.04 per Å³ in the Brillouin zone.^[17] The cell parameters and atomic positions are further optimized using the quasi-Newton method.^[18] The convergence thresholds between optimization cycles for convergence of energy, force, stress, and displacement are set as 5.0×10^{-6} eV per atom, 0.01 eV per Å, 0.02 GPa, and 5.0×10^{-4} Å, respectively. Based on the optimized geometry structure, the electronic structures are calculated and then the refractive indices (*n* and the birefringence Δn) are obtained. The shortest SHG output wavelength λ_{PM} is calculated based on the dispersion curves of refractive indices (e.g., n_o and n_e), satisfying the condition of $n_o(2\lambda_{\text{PM}}) = n_e(\lambda_{\text{PM}})$.^[19] Meanwhile, the SHG coefficients d_{ij} are calculated using following expression (1) developed by Lin et al.^[20]

$$\chi^{a\beta\gamma} = \chi^{a\beta\gamma}(\text{VE}) + \chi^{a\beta\gamma}(\text{VH}) + \chi^{a\beta\gamma}(\text{two bands}) \quad (1)$$

where $\chi^{a\beta\gamma}(\text{VE})$, $\chi^{a\beta\gamma}(\text{VH})$, and $\chi^{a\beta\gamma}(\text{two bands})$ denote the contributions from virtual-electron (VE) processes, virtual-hole (VH) processes, and two-band processes, respectively. The formulae for calculating $\chi^{a\beta\gamma}(\text{VE})$, $\chi^{a\beta\gamma}(\text{VH})$, and $\chi^{a\beta\gamma}(\text{two bands})$ are given as follows^[20]:

$$\chi^{a\beta\gamma}(\text{VH}) = \frac{e^3}{2\hbar^2 m^3} \times \sum_{v'c} \int \frac{d^3k}{4\pi^3} P(a\beta\gamma) \text{Im} \left[p_{vv'}^a p_{v'c}^\beta p_{cv}^\gamma \right] \left(\frac{1}{\omega_{cv}^3 \omega_{v'c}^2} + \frac{2}{\omega_{vc}^4 \omega_{c'v}^4} \right)$$

$$\chi^{a\beta\gamma}(\text{VE}) = \frac{e^3}{2\hbar^2 m^3} \times \sum_{v'c} \int \frac{d^3k}{4\pi^3} P(a\beta\gamma) \text{Im} \left[p_{vc}^a p_{v'c}^\beta p_{c'v}^\gamma \right] \left(\frac{1}{\omega_{cv}^3 \omega_{v'c}^2} + \frac{2}{\omega_{vc}^4 \omega_{c'v}^4} \right) \quad (2)$$

$$\chi^{a\beta\gamma}(\text{two bands}) = \frac{e^3}{2\hbar^2 m^3} \times \sum_{vc} \int \frac{d^3k}{4\pi^3} P(a\beta\gamma) \frac{\text{Im} \left[p_{vc}^a p_{c'v}^\beta (p_{vv}^\gamma - p_{cc}^\gamma) \right]}{\omega_{vc}^5}$$

Here a , β , and γ are Cartesian components, v and v' denote valence bands, and c and c' denote conduction bands. $P(a\beta\gamma)$ denotes full permutation and explicitly shows the Kleinman symmetry of the SHG coefficients. The band energy difference and momentum matrix elements are denoted as $\hbar\omega_{ij}$ and p_{ij}^a , respectively, and they are all implicitly k dependent. It is noted that the refractive indices and SHG coefficients can be accurately obtained by DFT in principle because these optical properties are determined by the virtual electronic excited processes, which are described by the first and second order perturbations on the ground state wave functions, respectively.

It should be emphasized that generalized gradient approximation (GGA) method with PBE functional usually heavily underestimates the energy bandgap E_g ^[21] while the hybrid PBE0 method^[22] can make an accurate prediction for most of the UV and deep-UV borates.^[23] Herein, the scissors-corrected GGA-PBE method is employed to calculate the optical properties,^[24] where the scissors operator is set as the difference between the PBE0 and GGA-PBE bandgaps. This self-consistent ab initio approach has been proven to be an efficient way without introducing any experimental parameter for investigating the structures and NLO properties in many types of NLO materials including KBBF, BPO₄, and other NLO borates and phosphates.^[9]

The structural evolution from BPO₄ to PBO₃O and PB₃O₆O (stage I) is proposed as demonstrated in Figure 1 based on the theoretical modeling and simulations. The optimized structures of PBO₃O and PB₃O₆O with space group symmetry of $P3_1c$ (C_{3v}) are shown in Figure 1b and c (for details see Table S1, Supporting Information). In stage I, $(\text{BO}_4)^{5-}$

tetrahedra are replaced by $(\text{BO}_3)^{3-}$ triangles, each of which is corner-shared with three $(\text{PO}_4)^{3-}$ to form a 2D infinite $(\text{PBO}_3\text{O})_\infty$ layer perpendicular to the c -axis. The $(\text{PO}_4)^{3-}$ units are aligned in the same orientation with three shared O^{2-} in the layer and one dangling O^{2-} outside of the layer. As indicated by anionic group theory, the 2D-layered structure of PBO₃O could exhibit a larger optical birefringence than the 3D framework structure of BPO₄ whereas the dangling bonds of the terminal oxygen in $(\text{PO}_4)^{3-}$ might reduce the bandgap. The DFT results confirm the above hypothesis very well. Table 1 lists the calculated bandgap E_g , SHG coefficients d_{ij} , birefringence Δn , UV absorption edge λ_{UV} and shortest SHG wavelength λ_{PM} of PBO₃O, as well as the calculated and experimental values of BPO₄ and KBBF. Compared with PBO₄, the Δn of PBO₃O is indeed enlarged from 0.011 to 0.061 as the E_g reduces from 9.30 to 8.01 eV. Accordingly, it is possible to shift the SHG output wavelength close to the deep-UV edge ($\lambda_{\text{PM}} \approx 205$ nm) in PBO₃O. In order to further enhance the phase-matching ability, a feasible way is the use of $(\text{B}_3\text{O}_6)^{3-}$ with large π orbitals to replace $(\text{BO}_3)^{3-}$ with small π orbitals increasing the anisotropic strength along the a - b plane as displayed in Figure 1c. The unit cell of PB₃O₆O is similar to that of PBO₃O, just with a larger cell constant a (and b). This kind of acentric-layered structure should be more favorable to exhibit a larger optical birefringence than that of PBO₃O for the phase-matching process. The calculations (see Table 1) show that PB₃O₆O exhibits close E_g (or λ_{UV}) but larger Δn , thus promote it exhibiting a shorter phase-matching SHG output ($\lambda_{\text{PM}} \approx 175$ nm) into the deep-UV region.

Notably, it should be emphasized that by the combination of NLO material genome $(\text{BO}_3)^{3-}/(\text{B}_3\text{O}_6)^{3-}$ and $(\text{PO}_4)^{3-}$, the structures in stage I actually improve the phase-matching ability of BPO₄. However, they still exhibit weaker NLO capabilities than those of KBBF, either for λ_{UV} or λ_{PM} . These can be attributed to the imperfect $(\text{PO}_4)^{3-}$ unit, in which a dangling oxygen atom is harmful for the further enlargement of the deep-UV bandgap.^[25] Then, we propose the following structure evolution of stage II as shown in Figure 1d and e, where the trigonal bipyramidal $(\text{PO}_3\text{F}_2)^{3-}$ units, similar to $(\text{AlO}_3\text{F}_2)^{3-}$ units in BaAlBO₃F₂, are further introduced to replace the tetrahedral $(\text{PO}_4)^{3-}$ unit to more favor the layered structure and large bandgap.^[26] In this way, $(\text{BO}_4)^{5-}$ and $(\text{PO}_4)^{3-}$ tetrahedra are simultaneously replaced by $(\text{BO}_3)^{3-}$ triangles (or $(\text{B}_3\text{O}_6)^{3-}$ polar rings) and $(\text{PO}_3\text{F}_2)^{3-}$ trigonal bipyramids, both of which are aligned in a close orientation within the a - b plane. Each $(\text{BO}_3)^{3-}$ (or $(\text{B}_3\text{O}_6)^{3-}$) is corner-shared with three $(\text{PO}_3\text{F}_2)^{3-}$ to form a 2D infinite $(\text{PBO}_3\text{F}_2)_\infty$ (or $(\text{PB}_3\text{O}_6\text{F}_2)_\infty$) layer perpendicular to the c -axis with two dangling F atoms above and below the plane. It is worth noting that these staggered layers are dense-stacking and very favorable to have a large anisotropy for NLO effect. Considering the eliminated nonbonding states of the anionic units, PBO₃F₂ and PB₃O₆F₂ are expected to be well transparent in the deep-UV region. The calculated E_g , d_{ij} , Δn , λ_{UV} , and λ_{PM} are listed in Table 1. It can be found that compared with PBO₃O (or PB₃O₆O), PBO₃F₂ (or PB₃O₆F₂) exhibits 1) wider E_g (≈ 9.2 and 9.1 eV) and shorter λ_{UV} (≈ 135 and 137 nm), close to those of BPO₄ (9.3 eV and 134 nm); 2) smaller d_{ij} (≈ 0.61 and 0.45 pm V^{-1}), but still larger than d_{11} (≈ 0.41 pm V^{-1}) of KBBF; and 3) larger Δn (≈ 0.08 and 0.10) and shorter λ_{PM} (≈ 155 and 137 nm), thus exhibiting better deep-UV phase-matching abilities.

Table 1. Calculated energy bandgap E_g , SHG coefficients d_{ij} , refractive indices n_o , n_e , birefringence Δn at 400 nm, UV absorption edge λ_{UV} and shortest SHG wavelength λ_{PM} of PBO_3O , PB_3O_6O , PBO_3F_2 and $PB_3O_6F_2$, as well as BPO_4 and $KBBF$.

		E_g (eV)	d_{ij} (pm V ⁻¹)	n_o	n_e	Δn	λ_{UV} (nm)	λ_{PM} (nm)
PBO_3O	Cal.	8.01	$d_{22}=0.82$; $d_{33}=0.94$	1.5031	1.4428	0.061	156	205
PB_3O_6O	Cal.	7.94	$d_{22}=0.45$; $d_{33}=0.36$	1.4081	1.3315	0.077	157	175
PBO_3F_2	Cal.	9.21	$d_{22}=0.61$	1.4660	1.3899	0.076	135	155
$PB_3O_6F_2$	Cal.	9.10	$d_{22}=0.45$	1.4030	1.3039	0.099	137	137
BPO_4	Cal.	9.30	$d_{36}=0.72$	1.5905	1.5789	0.011	134	N/A
	Exp. (ref. [5])	9.28	$d_{36}=0.76$	1.6059	1.6117	0.006	134	N/A
$KBBF$	Cal.	8.31	$d_{11}=0.41$	1.4787	1.4197	0.059	150	172
	Exp. (ref. [2])	8.45	$d_{11}=0.45$	1.4915	1.4035	0.088	147	161

Specifically, the λ_{PM} of PBO_3F_2 has been blue-shifted to 155 nm, shorter than that of $KBBF$ (≈ 161 nm), and the λ_{PM} of $PB_3O_6F_2$ can reach to its deep-UV absorption edge (≈ 137 nm), which is the shortest output wavelength for deep-UV SHG so far and can fill the gap of deep-UV all-solid-state laser ranging from 130 to 150 nm.^[4,27]

For PBO_3F_2 and $PB_3O_6F_2$, we further investigate their phase-matching characteristics and frequency conversion efficiency systematically, thus highlighting their practical capabilities for the deep-UV output, such as the sixth harmonic generation of the Nd: YAG lasers, since they are possible to go beyond $KBBF$. As shown in **Figure 2**, the type-I SHG phase-matching angles are determined for the fundamental wavelengths from 1100 to 274 nm. The Sellmeier equations of PBO_3F_2 and $PB_3O_6F_2$ are obtained by fitting the refractive indices (see Supporting Information), which are accurate enough in the UV and deep-UV regions from 137 to 400 nm. For the important 177.3 nm SHG output, the phase-matching angles θ for PBO_3F_2 and $PB_3O_6F_2$ are about 60.8 and 48.5°, respectively, while for $KBBF$ it

is about 69°. ^[5] In the practical type-I phase-matching process ($o + o \rightarrow e$), the effective SHG coefficient $d_{eff} = d_{22} \times \cos\theta \times \sin 3\psi$ according to the symmetry, where $\sin 3\psi$ can be tuned in the actual situation. As a result, the d_{eff} of PBO_3F_2 and $PB_3O_6F_2$ for 177.3 nm output are about 2.2 and 2.0 times larger than that of $KBBF$, respectively. The SHG conversion efficiency η is given approximately by

$$\eta = \frac{P_{2\omega}}{P_{\omega}} = \frac{8\pi^2 d_{eff}^2 L^2 I_{\omega}}{\epsilon_0 n_{\omega}^2 n_{2\omega} c \lambda_{\omega}^2} \quad (3)$$

where d_{eff} is the effective SHG coefficient, L is the length of a crystal, I_{ω} is the peak power density of the input beam, P_{ω} ($P_{2\omega}$) is the power of the fundamental (SHG) wave, ϵ_0 is the vacuum permittivity, n_{ω} and $n_{2\omega}$ are the refractive indices at the fundamental λ_{ω} (354.7 nm) and the SHG $\lambda_{2\omega}$ (177.3 nm) along the phase-matching direction, c represents the speed of light in vacuum. It can be deduced that under the same laser input conditions (e.g., I_{ω} , λ_{ω}) and crystal quality (e.g., L), the SHG conversion efficiency η of PBO_3F_2 and $PB_3O_6F_2$ crystals are about four times larger than that of $KBBF$. Considering that $KBBF$ -based device (i.e., the optically contacted $KBBF$ - CaF_2 prism-coupling device) has achieved the applicable deep-UV 6HG output (177.3 nm) of practical Nd: YAG 1064 nm laser with 200 mW power,^[2b] in principle the similar devices based on PBO_3F_2 and $PB_3O_6F_2$ crystals are capable of generating the same output with higher power (≈ 1 W), which would satisfy the urgent requirement for some industrial applications (e.g., lithography).

It should be noted that there are no interlayer cations in PBO_3F_2 and $PB_3O_6F_2$, thus making the layered structures more dense-stacked (e.g., the interlayer distance of $PB_3O_6F_2$ is only about 4.2 Å), and improving the capability for the deep-UV NLO harmonic generation. Since we have systemically evaluated the deep-UV NLO capabilities of PBO_3F_2 and $PB_3O_6F_2$, it is essential to show their structural stabilities as the practical materials that can be obtained in experiments. Firstly, the phonon spectra of PBO_3F_2 and $PB_3O_6F_2$ bulks along all the high symmetry lines in the Brillouin zone are calculated by the first-principles linear response methods.^[28] As shown in **Figure 3**, the dynamical stabilities are approved because no imaginary phonon mode

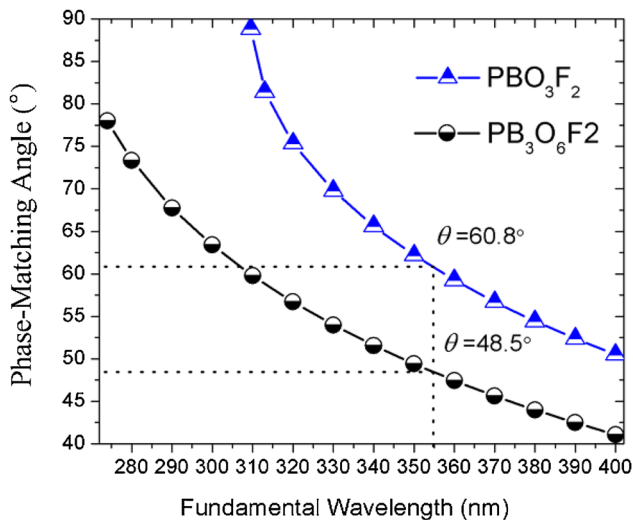


Figure 2. Type-I phase-matching angles with respect to fundamental wavelength of PBO_3F_2 and $PB_3O_6F_2$.

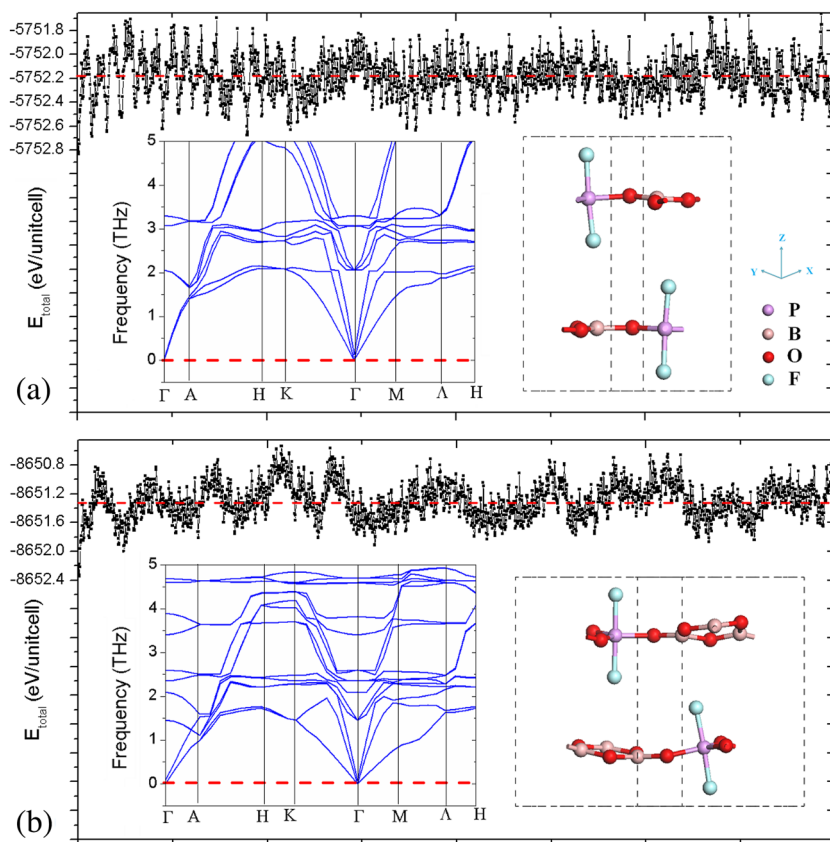


Figure 3. Phonon spectra, evolution of total energies and structures after the long-time MD simulations of PBO_3F_2 (a) and $\text{PB}_3\text{O}_6\text{F}_2$ (b).

emerges. Secondly, the full elastic tensors c_{ij} of PBO_3F_2 and $\text{PB}_3\text{O}_6\text{F}_2$ are determined using the finite strain technique based on first-principles calculations to further confirm the Born criterion for the two lattices to be stable.^[29] From the results (for PBO_3F_2 , $c_{11} = 105.9$, $c_{33} = 14.3$, $c_{44} = 6.2$, $c_{12} = 20.1$, $c_{13} = -2.1$; for $\text{PB}_3\text{O}_6\text{F}_2$, $c_{11} = 73.7$, $c_{33} = 12.6$, $c_{44} = 1.6$, $c_{12} = 1.8$, $c_{13} = -2.7$, unit: GPa), it is easy to verify that the general conditions for stability ($(c_{11} + c_{12}) \times c_{33} - 2 \times c_{13}^2 > 0$ and $(c_{11} - c_{12}) \times c_{44} > 0$) are satisfied.^[30] In the meantime, the first-principles molecular dynamics (MD) simulations are performed to verify the lattice structures of PBO_3F_2 and $\text{PB}_3\text{O}_6\text{F}_2$ are stable at room temperature (see Figure 3). The results show that the total energies with respect to time oscillate around the average value (red line), and their structures are maintained after long-time MD simulations (≈ 2 ps). Since PBO_3F_2 and $\text{PB}_3\text{O}_6\text{F}_2$ are stable in ambient condition, we suggest possible experimental program is to synthesize by new flux systems or synthesis methods to reduce the viscosity of the melt during the process of synthesis. Low temperature flux method maybe suitable for the synthesis of the fluorine borophosphates based on the reported study of $\text{NH}_4\text{BPO}_4\text{F}$.^[31] In the synthesis, one could also reduce the proportion of A-site cations and maximize the weight of boron, phosphorus, and fluorine suitably so that the fluorine borophosphate frameworks are prone to be constructed.

In fact, there are also some other structures with different symmetries according to the proposed design strategy. For

example, we can design the so-called β -phase with ABC stacking of $R3$ space group instead of the α -phase with AB stacking of $P62c$ mentioned above. As a comparison with α -phases, the β -phases of PBO_3F_2 and $\text{PB}_3\text{O}_6\text{F}_2$ exhibit higher total energies but close deep-UV NLO capabilities including energy bandgaps, SHG effects, birefringence, and the phase-matching outputs (for details see Figure S1 and Table S2, Supporting Information). Besides, another γ -phase of $\text{PB}_3\text{O}_6\text{F}_2$ with lower symmetry (Cc), which is similar to the $\text{NH}_4\text{B}_4\text{O}_6\text{F}$ (ABF) layered framework but without A-site NH_4^+ cations (see Figure S2 and Table S3, Supporting Information),^[14b] can still exhibit excellent deep-UV NLO capability with wide E_g (≈ 8.2 eV), strong d_{11} (≈ 0.70 pm V^{-1}), large Δn (≈ 0.09), and promising λ_{PM} (≈ 152 nm). No matter what phases can be obtained from the experiments, we provide a rational strategy to design a NLO structure with better deep-UV phase-matching SHG capability by combining the NLO material genome, which would promote the search for new deep-UV NLO materials with enhanced phase-matching abilities especially in the borophosphate system.

Finally, we discuss possible applications using PBO_3F_2 and $\text{PB}_3\text{O}_6\text{F}_2$, including those cannot be realized by KBBF. Above all, both of them can be used as the devices for deep-UV output of 193.7 and 177.3 nm, which have

important applications in photolithography, photoemission electron microscopy, and super-high-resolution photoemission spectrograph. In particular, for the $\text{PB}_3\text{O}_6\text{F}_2$ crystal, it is able to realize the fourth harmonic generation output (158.2 nm) of He-Ne laser, fifth harmonic generation output (138.9 nm) of ruby laser, and tunable deep-UV generation from 137 to 200 nm using Ti-sapphire laser. This means that it is superior to KBBF and could fill the gap of deep-UV all-solid-state laser between 100 and 150 nm, which will provide more powerful laser resources for future basic research and technology needs of materials science.^[2] In addition, since PBO_3F_2 and $\text{PB}_3\text{O}_6\text{F}_2$ are both van der Waals layered structures, they are possible to be further cleaved as 2D materials. The computational analysis shows that their monolayers can keep the deep-UV NLO capabilities of their bulk crystals very well with close SHG effects and wide transparent window from 0.14 to $3 \mu\text{m}$. Thus, they might be applied in some optical film devices with available NLO or photoelastic effect.^[32]

In conclusion, based on the chemical combination and structural evolution from a unique 3D BPO_4 framework to the dense-stacking layered structures, a series of borophosphates with excellent deep-UV NLO capabilities beyond KBBF are theoretically predicted using DFT modeling and simulations. The results demonstrate that they exhibit very large energy bandgaps, strong SHG effects, and moderate birefringence in the deep-UV region. Among them, PBO_3F_2 and $\text{PB}_3\text{O}_6\text{F}_2$ are

able to achieve the deep-UV SHG output with shorter phase-matching wavelengths (≈ 155 and 137 nm) than that of KBBF (≈ 161 nm) and higher frequency conversion efficiency for practical 177.3 nm output. In particular, the novel layered structure of $PB_3O_6F_2$ could produce the very short phase-matching deep-UV SHG coherent light of 137 nm, which would provide more powerful laser resources for scientists to reveal unprecedented details in novel solid-state materials.

Supporting Information

Supporting Information is available from the Wiley Online Library or from the author.

Acknowledgments

This work was supported by the NSFC Grant Nos. 11574024, 91622118 and NSAF U1530401. F. Liu acknowledges support from US DOE-BES (No. DE-FG02-04ER46148). Z. Lin acknowledges support from outstanding member in Youth Innovation Promotion Association at CAS.

Conflict of Interest

The authors declare no conflict of interest.

Keywords

deep-ultraviolet, first-principles calculations, nonlinear optical crystals, phase-matching, second harmonic generation

Received: June 1, 2018

Revised: June 8, 2018

Published online:

- [1] a) T. Sekikawa, A. Kosuge, T. Kanai, S. Watanabe, *Nature* **2004**, 432, 605; b) U. Eismann, M. Scholz, T. Paasch-Colberg, J. Stuhler, *Laser Focus World* **2016**, 52, 39.
- [2] a) C. Chen, G. Wang, X. Wang, Z. Xu, *Appl. Phys. B: Lasers Opt.* **2009**, 97, 9; b) B. Xu, L. Liu, X. Wang, C. Chen, X. Zhang, S. Lin, *Appl. Phys. B: Lasers Opt.* **2015**, 121, 489.
- [3] W. Zhang, H. Yu, H. Wu, P. Halasyamani, *Chem. Mater.* **2017**, 29, 2655.
- [4] T. Tran, H. Yu, J. Rondinelli, K. Poeppelmeier, P. Halasyamani, *Chem. Mater.* **2016**, 28, 5238.
- [5] Z. Li, Z. Lin, Y. Wu, P. Fu, Z. Wang, C. Chen, *Chem. Mater.* **2004**, 16, 2906.
- [6] X. Zhang, L. Wang, S. Zhang, G. Wang, S. Zhao, Y. Zhu, Y. Wu, C. Chen, *J. Opt. Soc. Am. B* **2011**, 28, 2236.
- [7] C. Chen, Z. Lin, Z. Wang, *Appl. Phys. B: Lasers Opt.* **2005**, 80, 1.
- [8] A. Jain, S. Ong, G. Hautier, W. Chen, W. Richards, S. Dacek, S. Cholia, D. Gunter, D. Skinner, G. Ceder, K. Persson, *APL Mater.* **2013**, 1, 011002.
- [9] a) C. Chen, Y. Wang, B. Wu, K. Wu, W. Zeng, L. Yu, *Nature* **1995**, 373, 322; b) L. Kang, S. Luo, H. Huang, N. Ye, Z. Lin, J. Qin, C. Chen, *J. Phys. Chem. C* **2013**, 117, 25684; c) Z. Lin, X. Jiang, L. Kang, P. Gong, S. Luo, M. Lee, *J. Phys. D: Appl. Phys.* **2014**, 47, 253001; d) L. Kang, S. Luo, G. Peng, N. Ye, Y. Wu, C. Chen, Z. Lin, *Inorg. Chem.* **2015**, 54, 10533; e) L. Kang, M. Zhou, J. Yao, Z. Lin, Y. Wu, C. Chen, *J. Am. Chem. Soc.* **2015**, 137, 13049.
- [10] C. Chen, B. Wu, A. Jiang, G. You, *Sci. Sin. B* **1985**, 28, 235.
- [11] C. Chen, Y. Wu, A. Jiang, B. Wu, G. You, R. Li, S. Lin, *J. Opt. Soc. Am. B* **1989**, 6, 616.
- [12] Y. Xia, C. Chen, D. Tang, B. Wu, *Adv. Mater.* **1995**, 7, 79.
- [13] C. Chen, N. Ye, J. Lin, J. Jiang, W. Zeng, B. Wu, *Adv. Mater.* **1999**, 11, 1071.
- [14] a) R. Cong, Y. Wang, L. Kang, Z. Zhou, Z. Lin, T. Yang, *Inorg. Chem. Front.* **2015**, 2, 170; b) G. Shi, Y. Wang, F. Zhan, B. Zhang, R. Yang, X. Hou, S. Pan, K. Poeppelmeier, *J. Am. Chem. Soc.* **2017**, 139, 10645; c) F. Liang, L. Kang, P. Gong, Z. Lin, Y. Wu, *Chem. Mater.* **2017**, 29, 7098.
- [15] a) M. Payne, M. Teter, D. Allan, T. Arias, J. Joannopoulos, *Rev. Mod. Phys.* **1992**, 64, 1045; b) S. Clark, M. Segall, C. Pickard, P. Hasnig, M. Probert, K. Refson, M. Payne, *Z. Kristallogr.* **2005**, 220, 567.
- [16] A. Rappe, K. Rabe, E. Kaxiras, J. Joannopoulos, *Phys. Rev. B* **1990**, 41, 1227.
- [17] H. Monkhorst, J. Pack, *Phys. Rev. B* **1976**, 13, 5188.
- [18] B. Pfrommer, M. Cote, S. Louie, M. Cohen, *J. Comput. Phys.* **1997**, 131, 233.
- [19] R. Boyd, *Nonlinear Optics*, 3rd ed., Academic Press, Cambridge, Massachusetts, USA **2008**, p. 79.
- [20] J. Lin, M. Lee, Z. Liu, C. Chen, C. Pickard, *Phys. Rev. B* **1999**, 60, 13380.
- [21] J. Perdew, K. Burke, M. Ernzerhof, *Phys. Rev. Lett.* **1996**, 77, 3865.
- [22] C. Adamo, V. Barone, *J. Chem. Phys.* **1999**, 110, 6158.
- [23] Z. Lin, L. Kang, T. Zheng, R. He, H. Huang, C. Chen, *Comput. Mater. Sci.* **2012**, 60, 99.
- [24] a) M. Levy, J. Perdew, V. Sahni, *Phys. Rev. A* **1984**, 30, 2745; b) R. Godby, M. Schluter, L. Sham, *Phys. Rev. B* **1988**, 37, 10159.
- [25] R. He, H. Huang, L. Kang, W. Yao, X. Jiang, Z. Lin, J. Qin, C. Chen, *Appl. Phys. Lett.* **2013**, 102, 231904.
- [26] Z. Hu, M. Yoshimura, K. Muramatsu, Y. Mori, T. Sasaki, *Jpn. J. Appl. Phys. Pt. 2-Lett.* **2002**, 41, L1131.
- [27] X. Jiang, S. Luo, L. Kang, P. Gong, H. Huang, S. Wang, Z. Lin, C. Chen, *ACS Photonics* **2015**, 2, 1183.
- [28] Y. Yao, J. Tse, J. Sun, D. Klug, R. Martonak, T. Iitaka, *Phys. Rev. Lett.* **2009**, 102, 9601.
- [29] B. Karki, G. Ackland, J. Crain, *J. Phys.: Condens. Matter* **1997**, 9, 8579.
- [30] R. Cowley, *Phys. Rev. B* **1976**, 13, 4877.
- [31] M. Li, W. Liu, M. Ge, H. Chen, X. Yang, J. Zhao, *Chem. Commun.* **2004**, 11, 1272.
- [32] a) X. X. Jiang, S. Y. Luo, L. Kang, P. F. Gong, W. J. Yao, H. W. Huang, W. Li, R. J. Huang, W. Wang, Y. C. Li, X. D. Li, X. Wu, P. X. Lu, L. F. Li, C. T. Chen, Z. S. Lin, *Adv. Mater.* **2015**, 27, 4851; b) G. Eda, S. A. Maier, *ACS Nano* **2013**, 7, 5660.